Heme Oxygenase-1 Regulates Ferrous Iron and Foxo1 in Control of Hepatic Gluconeogenesis

Wang Liao, Wanbao Yang, Zheng Shen, Weiqi Ai, Quan Pan, Yuxiang Sun, and Shaodong Guo

Diabetes 2021;70:696–709 | https://doi.org/10.2337/db20-0954

The liver is a key player for maintaining glucose homeostasis. Excessive hepatic glucose production is considered to be a key for the onset of type 2 diabetes. The primary function of heme oxygenase-1 (HO1) is to catalyze the degradation of heme into biliverdin, ferrous iron, and carbon monoxide. Previous studies have demonstrated that the degradation of heme by HO1 in the liver results in mitochondrial dysfunction and drives insulin resistance. In this study, by overexpressing HO1 in hepatocytes and mice, we showed that HO1 promotes gluconeogenesis in a Foxo1-dependent manner. Importantly, HO1 overexpression increased the generation of ferrous iron in the liver, which further activates nuclear factor-κB and phosphorylates Foxo1 at Ser273 to enhance gluconeogenesis. We further assessed the role of HO1 in insulin-resistant liver-specific knockout of IRS1 and IRS2 genes (L-DKO) mice, which exhibit upregulation of HO1 in the liver and hepatic ferrous iron overload. HO1 knockdown by shRNA or treatment of iron chelator rescued the aberrant gluconeogenesis in L-DKO mice. In addition, we found that systemic iron overload promotes gluconeogenesis by activating the hepatic protein kinase A→Foxo1 axis. Thus, our results demonstrate the role of HO1 in regulating hepatic iron status and Foxo1 to control gluconeogenesis and blood glucose.

METABOLISM

Understanding the pathophysiology of type 2 diabetes (T2D) is critical for us to find approaches in control of this disease, and it is known that diabetic hyperglycemia results from defective insulin action in company with hyperglucagonemia (1). The liver is an important organ that can respond to both insulin and glucagon upon nutrient availability in control of hepatic glucose production (HGP) (2). Glucagon and insulin reciprocally control glucose homeostasis, which requires tight control of gene transcription in order to exert the opposite effects on glucose homeostasis (3,4).

As a member of *O*-class forkhead/winged helix transcriptional factor, Foxo1 is a key player in the transcriptional regulation of hepatic glucose metabolism (3). It was found that in the insulin-signaling protein kinase B (Akt) activation triggers the phosphorylation of Foxo1 at Ser256 in humans, equivalent to Ser253 in mice; this drives Foxo1 nuclear exportation and ubiquitination (5). By contrast, we recently discovered that glucagon promotes Foxo1 nuclear translocation by phosphorylating Foxo1 at Ser276 in humans and activates transcriptions of rate-limiting gluconeogenic genes (6). Given the dual roles of Foxo1 in regulating HGP and eventually controlling glucose homeostasis, Foxo1 is believed to be a potential target for the treatment of T2D (7).

In addition to gluconeogenic genes, Foxo1 also regulates other target genes (8–10), one of which, heme oxygenase-1 (HO1), has attracted attention in recent years (11). HO1 catalyzes the degradation of heme into biliverdin, ferrous iron, and carbon monoxide. Historically, HO1 is considered as an anti-inflammatory molecule in different tissues due to the effects of carbon monoxide and bilirubin (converted from biliverdin) (11). Moreover, the transcription of HO1 is regulated by the redox-sensitive transcription factor Nrf2, which binds to the antioxidant response element in the upstream promoter of HO1 (12). Thus, HO1 is also considered to be antioxidant. As reported, induction of HO1 ameliorates hyperglycemia in nonobese insulin-resistant rats (13). Paradoxically, overexpression of HO1 in adipose tissue failed to protect the mice from diet-induced insulin resistance (14). Furthermore, a recent report indicated that liver-specific HO1 knockout protected

Department of Nutrition, College of Agriculture and Life Sciences, Texas A&M University, College Station, TX

Corresponding author: Shaodong Guo, shaodong.guo@tamu.edu

Received 22 September 2020 and accepted 15 December 2020

This article contains supplementary material online at https://doi.org/10.2337/figshare.13382714.

mice against high-fat diet–induced insulin resistance (15). We have also reported that hepatic Foxo1-induced HO1 upregulation results in mitochondrial dysfunction, which further leads to insulin resistance (16). These findings, which are opposite to the historical view, impelled us to further explore the role of HO1 in hepatic glucose metabolism.

In the current study, we investigated the roles of HO1 in hepatic gluconeogenesis by overexpression or suppression of HO1 in hepatocytes and mouse liver. We found that HO1 regulates HGP via Foxo1, associated metabolic inflammation, and excessive ferrous iron.

RESEARCH DESIGN AND METHODS

Animals

The transgenic mice carrying Foxo1 floxed alleles ($Foxo1^{fl/fl}$) and IRS1/IRS2 floxed alleles ($IRS1^{fl/fl}$::$IRS2^{fl/fl}$) were bred with the albumin-Cre mice to generate the liver-specific Foxo1 knockout (L-FKO) mice, as well as liver-specific IRS1 and IRS2 knockout (L-DKO) mice, respectively (17,18). Foxo1-S273A knockin ($Foxo1\text{-}S273^{A/A}$) mice were generated using the CRISPR/Cas9 approach as described previously (6). All of the mice generated were based on the background of C57BL/6. Male mice (8–12 weeks old) were used for the study and were fed a standard chow diet ad libitum. The animal protocol was approved by the Institutional Animal Care and Use Committee at Texas A&M University.

Cell Culture

Primary hepatocytes were isolated from 8- to 12-week-old male mice and cultured in DMEM with 10% FBS as described previously (17,19). The cells were transfected with adenovirus expressing GFP (Adv-GFP) or Adv-HO1 (VectorBuilder, Chicago, IL) for 17–24 h in specific experiments. The p65 inhibitor JSH23 (Sigma-Aldrich, St. Louis, MO) or iron chelator deferoxamine mesylate (DFO) (Sigma-Aldrich) was used to treat cells for 0.5 h prior to the transfection of adenovirus in the corresponding experiment. In the experiments with siRNA transfection, hepatocytes were transfected with 80 pmol of specific siRNA by Lipofectamine 3000 (Invitrogen, Carlsbad, CA) for 12 h and then transfected with Adv-GFP or Adv-HO1.

HGP Assay

Primary hepatocytes were transfected with Adv-GFP or Adv-HO1 for 20 h and then cultured in the HGP buffer (120 mmol/L NaCl, 5.0 mmol/L KCl, 2.0 mmol/L $CaCl_2$, 25 mmol/L $NaHCO_3$, 2.5 mmol/L KH_2PO_4, 2.5 mmol/L $MgSO_4$, 10 mmol/L HEPES, 0.5% BSA, 10 mmol/L sodium DL-lactate, and 5 mmol/L pyruvate, pH 7.4) for 3 h with or without 100 nmol/L glucagon. The culture medium was collected to assess HGP using the Amplex Red glucose assay kit (Invitrogen).

Adeno-Associated Virus 8–Mediated Gene Delivery

The open reading frame sequence of GFP or HO1 was cloned into an adeno-associated virus 8 (AAV8) vector. AAV8-GFP or AAV8-HO1 was generated from these plasmids by VectorBuilder and then injected once into 8- to 12-week-old male mice via retro-orbital at the concentration of 10^{11} genome copies/mouse. Blood glucose was monitored using a glucometer (Danyer, Whippany, NJ). Pyruvate tolerance and glucagon tolerance tests were performed upon 16 h of fasting on days 8 and 11 post-injection of virus, respectively. Tissues were collected 14 days after the AAV8 injection. Serum insulin (catalog number 589501; Cayman Chemical) and glucagon (RAB0202; Sigma-Aldrich) levels, as well as liver triglyceride (catalog number ab65336; Abcam, Cambridge, MA) and cholesterol (catalog number ab65359; Abcam) levels, were measured by corresponding commercial kit. The activity of ALT in the serum sample was measured by a kit purchased from Sigma-Aldrich (catalog number MAK052).

Real-time PCR

Total RNA was extracted by TRIzol reagent (Invitrogen) and used for cDNA synthesis via the iScript cDNA Synthesis Kit (Bio-Rad Laboratories, Hercules, CA). The cDNA was amplified by a SYBR Green–based Master Mix (Bio-Rad Laboratories) on a CFX384 Touch Real-Time PCR detection system (Bio-Rad Laboratories). Cyclophilin was used as the housekeeping gene. Sequences of the primers are available in Supplementary Table 1 (15,17,20).

Western Blotting

Protein extracted from hepatocytes or liver tissues was loaded in SDS-PAGE and transferred onto a polyvinylidene difluoride membrane for Western blotting. Primary antibodies against HO1 (82206), Foxo1 (2880S), phosphorylated (p)Foxo1-S253 (9461S), pCREB-S133 (9198S), CREB (9197S), pIκkβ-S177/S181 (2078S), Iκkβ (2370S), pp65-S536 (3031S), p65 (8242S), pp38-T180/Y182 (CST 4511S), pAKT-S473 (9271S), Akt (9272S) β-actin (4970S), and GAPDH (CST 5174S) were purchased from Cell Signaling Technology (Danvers, MA). The antibody against p38α was purchased from ABclonal Technology (A14401; Woburn, MA). The antibody against pFoxo1-S273 was generated as previously described (6). The intensity of each band was analyzed by the ImageJ software (National Institutes of Health).

Cellular Superoxide Dismutase Activity

The activity of superoxide dismutase (SOD) in hepatocytes was evaluated by a colorimetric kit (Abcam) according to the manufacturer's manual. Briefly, hepatocytes isolated from wild-type mice were transfected with Adv-GFP or Adv-HO1 for 24 h. The cells were lysed and incubated with working solutions at 37°C for 20 min. The absorbance was read at 450 nm by a microplate reader.

Detection of Intracellular Reactive Oxygen Species

The reactive oxygen species (ROS) in hepatocytes was detected using MitoSOX Red mitochondrial superoxide indicator (Invitrogen). Hepatocytes isolated from wild-type mice were transfected with Adv-GFP or Adv-HO1

for 24 h. The cells were then incubated with 5 μmol/L MitoSOX reagent working solution for 10 min at 37°C. The ROS was visualized by confocal microscope (Leica Biosystems, Wetzlar, Germany).

Immunoprecipitation

Hepatocytes were lysed in TNE buffer (50 mmol/L Tris-HCl, 100 mmol/L NaCl, and 0.1 mmol/L EDTA, pH 7.4) with protease inhibitors and phosphatase inhibitors. The cell lysates were incubated with the antibody against Iκkβ (Cell Signaling Technology) overnight at 4°C. The immune complexes were then precipitated by the IgG-coated magnetic beads (Invitrogen) at 4°C for 4 h. The complexes were then denatured by boiling at 95°C for 5 min in SDS sample buffer.

Detection of Intracellular Ferrous Iron

The level of intracellular ferrous iron was assessed by FeRhoNox-1 fluorescent probe (Goryo Chemical Inc., Sapporo, Japan) according to the manual (21). Hepatocytes were transfected with Adv-GFP or Adv-HO1 for 24 h. The FeRhoNox-1 solution (5 μmol/L in 200 μL of Hanks' balanced salt solution) was then added to cells, followed by the incubation at 37°C for 1 h. Finally, the cells were visualized in Hanks' balanced salt solution by a confocal fluorescent microscope (Leica Biosystems).

Measurement of the Ferrous Iron Level in Liver Tissues

The content of ferrous iron in liver tissues was measured using an iron assay kit (ab83366; Abcam). Liver tissues were homogenized in the assay buffer and then incubated with or without iron reducer, followed by the incubation with the iron probe at 37°C for 1 h in the dark. The absorbance at 593 nm was read.

Iron-Dextran Treatment in Mice

Male (8–12 weeks old) $Foxo1^{fl/fl}$ or L-FKO mice were injected with saline or Iron-Dextran (Sigma-Aldrich) (22.5 mg/kg/injection) intravenously twice at an interval of 4 h (22). Pyruvate tolerance test was performed 24 h after the first injection of iron-dextran upon 16 h of fasting.

AAV8-Mediated HO1 Knockdown in L-DKO Mice

shRNA against HO1 was cloned into an AAV8 vector to generate HO1 shRNA by VectorBuilder. The AAV8-based shRNA was injected to $IRS1^{fl/fl}$::$IRS2^{fl/fl}$ or L-DKO mice (male, 8–12 weeks old) via retro-orbital at the concentration of 10^{11} genome copies/mouse. Pyruvate tolerance and glucose tolerance tests were performed upon 16 h of fasting on days 8 and 11 postinjection of virus, respectively. Tissues were collected 14 days after the AAV8 injection.

DFO Treatment in L-DKO Mice

Male (8–12 weeks old) $IRS1^{fl/fl}$::$IRS2^{fl/fl}$ or L-DKO mice were treated with 10 mg/kg body weight DFO (23) by intraperitoneal injection; they were then fasted for 14 h, followed by another injection of DFO with the same dosage. The fasting blood glucose was measured, and a pyruvate tolerance test was performed 2 h after the second injection of DFO.

Statistical Analyses

Results were presented as mean ± SEM of at least three independent experiments. The statistical analyses were performed with Prism 8 software (GraphPad, San Diego, CA). Two-tailed *t* tests were applied to data from two different groups. Data from more than two groups were analyzed by one-way or two-way ANOVA with Tukey post hoc test to determine the significance, as appropriate. $P < 0.05$ was considered as statistically different.

Data and Resource Availability

The data generated from this study and the associated resources are available from the corresponding author upon reasonable request.

RESULTS

HO1 Regulates Foxo1 and Promotes HGP in Hepatocytes

To examine the role of HO1 in HGP, we overexpressed HO1 in hepatocytes and found that HGP was increased 25.8% as a result of HO1 overexpression in hepatocytes isolated from the control mice; this was comparable to the effect of glucagon treatment (Fig. 1*A*). However, Adv-HO1 and glucagon did not show a synergistic effect in the HO1-overexpressed hepatocytes ($P = 0.5$); this suggests that HO1 overexpression and glucagon may promote HGP by targeting overlapping signaling pathways. In addition, HO1 overexpression improved the transcriptional level of Foxo1 target genes responsible for gluconeogenesis, including G6Pc (2.69-fold) and Pck (1.82-fold), but did not affect the mRNA level of Foxo1 (Fig. 1*B*).

Since Foxo1 integrates the glucagon/protein kinase A (PKA) signaling to enhance gluconeogenesis via phosphorylation at Ser273 (6), we then evaluated the effects of HO1 overexpression on Foxo1 phosphorylation. It was found that HO1 overexpression mimicked the effects of glucagon on activating PKA and Foxo1; this was evident by the increased levels of pCREB-S133 and pFoxo1-S273 and increased total Foxo1 of 1.42-fold, 2.16-fold, and 1.73-fold, respectively (Fig. 1*C*). Conversely, HO1 overexpression did not show a significant effect on HGP in the hepatocytes isolated from L-FKO or Foxo1 constitutive dephosphorylation $Foxo1\text{-}S273^{A/A}$ mice (Fig. 1*A* and *D*). Collectively, HO1 overexpression promotes HGP via the regulation of Foxo1 phosphorylation. In addition, HO1 overexpression in hepatocytes increased the mRNA level of proinflammatory genes, such as MCP1 and tumor necrosis factor-α (TNF-α) (Fig. 1*E*). Taken together, these data suggest a potential link between HO1 overexpression and enhanced HGP in hepatocytes.

HO1 Overexpression Activates Nuclear Factor-κB and Induces HGP in Hepatocytes

Since it was reported that HO1 drives metainflammation in mouse and human through nuclear factor-κB (NF-κB)

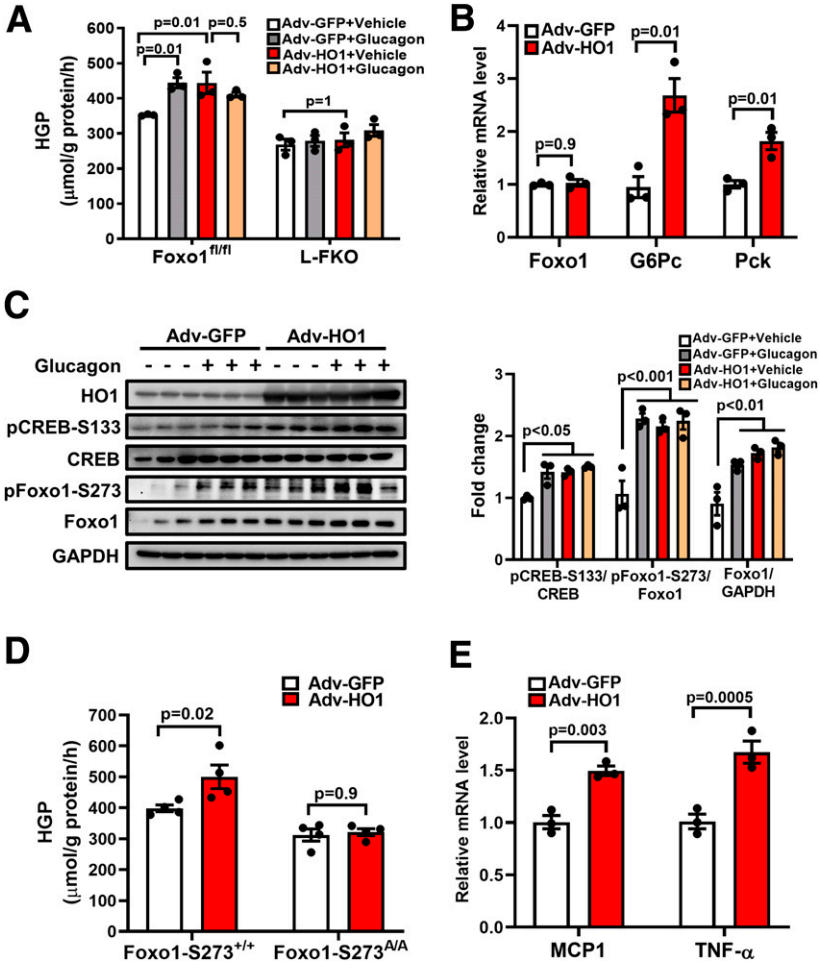

Figure 1— HO1 regulates Foxo1 to promote HGP in hepatocytes. *A*: Hepatocytes isolated from Foxo1$^{fl/fl}$ or L-FKO mice were transfected with Adv-GFP or Adv-HO1 for 20 h and then switched to HGP buffer for 3 h, with or without 100 nmol/L glucagon stimulation. HGP was normalized to total protein levels. $n = 3$/group. Results are presented as mean ± SEM. *B*: Hepatocytes from wild-type mice were isolated and transfected with Adv-GFP or Adv-HO1 for 24 h. Total RNA was extracted for quantitative PCR analyses to detect the levels of Foxo1, G6Pc, and Pck. The relative mRNA expression was normalized by cyclophilin. $n = 3$/group. Results are presented as mean ± SEM. *C*: Hepatocytes isolated from Foxo1$^{fl/fl}$ or L-FKO mice were transfected with Adv-GFP or Adv-HO1 for 20 h and then starved in DMEM with 1% FBS for 1 h, followed by 100 nmol/L glucagon stimulation for 3 h. The cell lysates were loaded onto a 10% SDS-PAGE for Western blotting to detect HO1, pCREB-S133, total CREB, pFoxo1-S273, and total Foxo1. The relative expression level of each protein was normalized to the corresponding GAPDH and quantified by ImageJ. $n = 3$/group. Results are presented as mean ± SEM. *D*: Hepatocytes from Foxo1-S273$^{+/+}$ (control) or Foxo1-S273$^{A/A}$ mice were isolated and transfected with Adv-GFP or Adv-HO1 for 20 h. The cells were then switched to HGP buffer for 3 h. HGP was normalized to total protein levels. $n = 4$/group. Results are presented as mean ± SEM. *E*: Hepatocytes isolated from wild-type mice were transfected with Adv-GFP or Adv-HO1 for 24 h. Total RNA was extracted for quantitative PCR analyses to detect the levels of MCP1 and TNF-α. The relative mRNA expression was normalized by cyclophilin. $n = 3$/group. Results are presented as mean ± SEM.

(15), we aimed to examine whether the activation of NF-κB by HO1 overexpression links to the induction of HGP. As shown in Fig. 2*A*, overexpression of HO1 in hepatocytes activated NF-κB by promoting the phosphorylation of p65 at Ser536. Notably, the transfection of p65 siRNA, or the treatment with p65 inhibitor JSH23, diminished the effects of HO1 overexpression on HGP by 25.0% and 17.1%, respectively (Fig. 2*B* and *C*). Although HO1 overexpression also increased the phosphorylation of proinflammatory p38 (Fig. 2*A*), neither p38 siRNA nor p38 inhibitor showed a significant influence in abolishing the effect of HO1 overexpression on HGP (Supplementary Fig. 1*A* and *B*).

It was also demonstrated that knockdown or blocking of p65 impaired the effects of HO1 overexpression on PKA→Foxo1 signaling (Fig. 2*D* and *E*). These results are consistent with the existing literature reporting the inhibition of PKA by the inactivation of hepatic p65/NF-κB (24). Hence, NF-κB mediates the effects of HO1 overexpression in activating the PKA→Foxo1 axis to promote HGP.

HO1 Overexpression Promotes Gluconeogenesis Dependent on Foxo1 In Vivo

We further aimed to demonstrate that HO1 regulates Foxo1 to promote gluconeogenesis in vivo. HO1 was overexpressed in male control or L-FKO mice by injecting

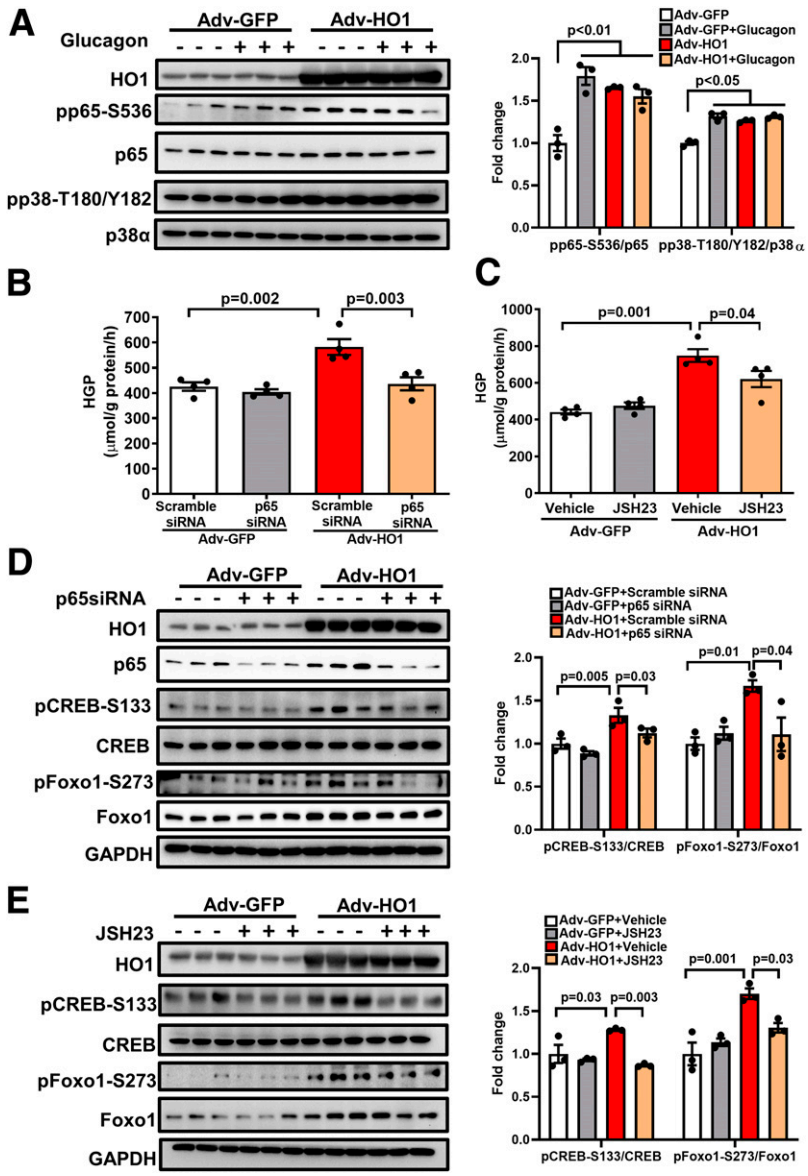

Figure 2—HO1 overexpression activates NF-κB and induces HGP in hepatocytes. *A*: Hepatocytes isolated from wild-type mice were transfected with Adv-GFP or Adv-HO1 for 16 h and then starved in DMEM with 1% FBS for 1 h, followed by 100 nmol/L glucagon stimulation for 1 h. The cell lysates were loaded onto a 10% SDS-PAGE for Western blotting to detect HO1, pp65-S536, total p65, pp38-T180/Y182, and total p38α. The relative expression of each phosphorylated protein was normalized to the corresponding total protein and quantified by ImageJ software. $n = 3$/group. Results are presented as mean ± SEM. *B*: Hepatocytes isolated from wild-type mice were transfected with scramble siRNA or p65 siRNA for 12 h and then transfected with Adv-GFP or Adv-HO1 for 24 h. Afterward, the cells were switched to HGP buffer for 3 h. HGP was normalized to total protein levels. $n = 4$/group. Results are presented as mean ± SEM. *C*: Hepatocytes isolated from wild-type mice were pretreated by 10 μmol/L p65 inhibitor JSH23 for 0.5 h and then transfected with Adv-GFP or Adv-HO1 for 20 h, followed by incubation in HGP buffer for 3 h. HGP was normalized to total protein levels. $n = 4$/group. Results are presented as mean ± SEM. *D*: Hepatocytes isolated from wild-type mice were transfected with scramble siRNA or p65 siRNA for 12 h and then transfected with Adv-GFP or Adv-HO1 for 24 h. The cell lysates were loaded onto a 10% SDS-PAGE for Western blotting to detect HO1, total p65, pCREB-S133, total CREB, pFoxo1-S273, and total Foxo1. The relative expression of each phosphorylated protein was normalized to the corresponding total protein and quantified by ImageJ. $n = 3$/group. Results are presented as mean ± SEM. *E*: Hepatocytes isolated from wild-type mice were pretreated by 10 μmol/L p65 inhibitor JSH23 for 0.5 h and then transfected with Adv-GFP or Adv-HO1 for 24 h. The cell lysates were loaded onto a 10% SDS-PAGE for Western blotting to detect HO1, total p65, pCREB-S133, total CREB, pFoxo1-S273, and total Foxo1. The relative expression of each phosphorylated protein was normalized to the corresponding total protein and quantified by ImageJ. $n = 3$/group. Results are presented as mean ± SEM.

AAV8-HO1. Fasting blood glucose of the control mice was significantly increased by AAV8-HO1 (AAV8-GFP 86.7 mg/dL vs. AAV8-HO1 104 mg/dL, $P = 0.007$) (Fig. 3*A*). Such an effect in the L-FKO mice was insignificant ($P = 0.2$) (Fig. 3*A*). Of note, HO1 overexpression elevated blood glucose under the feeding condition in both the control (AAV8-GFP 161.5 mg/dL vs. AAV8-HO1 191.1 mg/dL, $P = 0.002$) and L-FKO mice (AAV8-GFP 143.3 mg/dL vs.

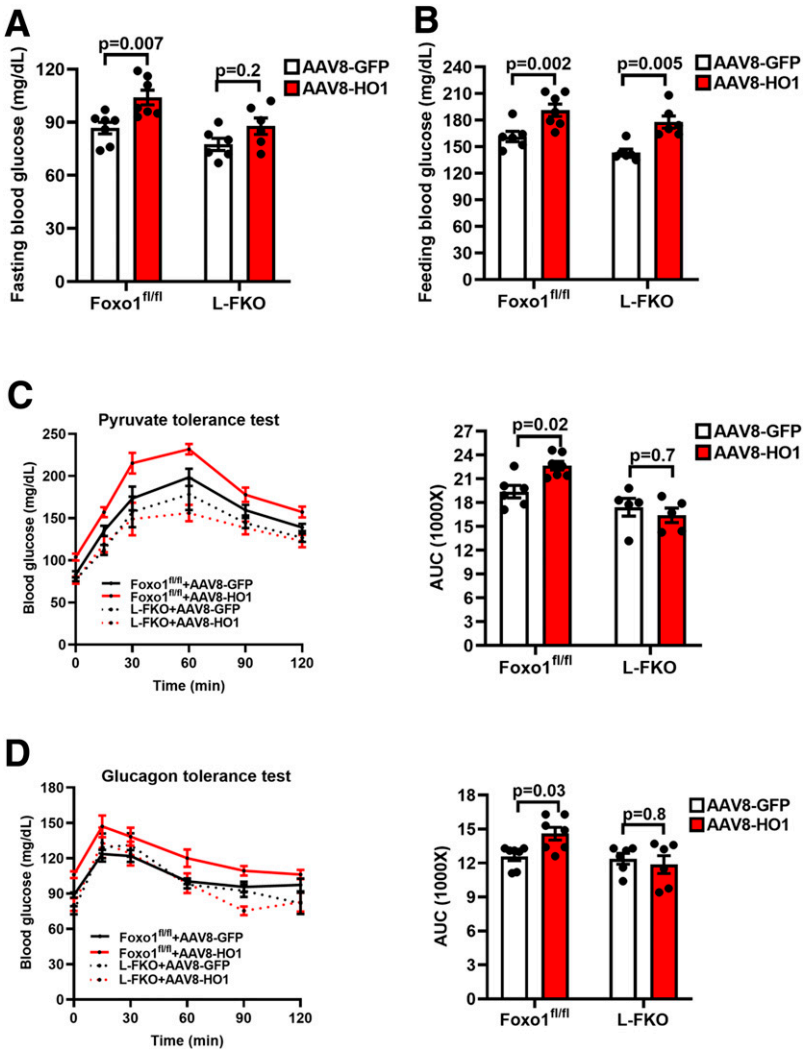

Figure 3—HO1 overexpression promotes gluconeogenesis dependent on Foxo1 in vivo. *A* and *B*: AAV8-GFP or AAV8-HO1 was delivered via retro-orbital to male mice (8–12 weeks old). Blood glucose after 16 h of fasting or underfeeding conditions was measured 8 days after the virus injection. $n = 4$–7 mice/group. Results are presented as mean ± SEM. *C* and *D*: AAV8-GFP or AAV8-HO1 was delivered via retro-orbital to male mice (8–12 weeks old) for 7 days. The mice were fasted for 16 h and then subjected to a 2-h pyruvate tolerance test (8 days postinjection, 2 g/kg body weight pyruvate i.p. injection) and glucagon tolerance test (11 days postinjection, 16 μg/kg body weight glucagon i.p. injection). The area under the curve (AUC) of each profile was calculated. $n = 5$–7 mice/group. Results are presented as mean ± SEM.

AAV8-HO1 177.8 mg/dL, $P = 0.005$) (Fig. 3*B*). The increase of feeding blood glucose implied the development of insulin resistance driven by HO1, which was also evidenced by the increased serum insulin concentration exhibited by the HO1-overexpressed mice (Supplementary Fig. 2*A*). In addition, HO1-overexpressed hepatocytes showed impaired response toward insulin stimulation (Supplementary Fig. 2*B*). These results further support a previous study that demonstrated the role of HO1 in driving insulin resistance (15).

To specify the roles of in vivo HO1 overexpression in promoting gluconeogenesis, we then performed pyruvate tolerance and glucagon tolerance tests. AAV8-HO1 increased glucose production in the 2-h time course pyruvate tolerance test in the control mice ($P = 0.02$), but not in the L-FKO mice ($P = 0.7$) (Fig. 3*C*). AAV8-HO1 exerted a similar effect in the glucagon tolerance test, in which the blood glucose profile of the control mice was significantly altered ($P = 0.03$) by HO1 overexpression, but not the L-FKO mice ($P = 0.8$) (Fig. 3*D*). Additionally, the control liver with HO1 overexpression displayed a higher level of pCREB-S133 (1.47-fold) than their littermates overexpressed by GFP (Fig. 4*A*); this led to increases in pFoxo1-S273 and total Foxo1 by 1.93-fold and 1.43-fold, respectively (Fig. 4*A*). The activation of Foxo1 consequently enhanced the transcriptions of gluconeogenic genes, including *G6Pc* and *Pck*, in the control mice instead of the L-FKO mice (Fig. 4*B*). Taken together, HO1 overexpression promotes gluconeogenesis in a Foxo1-dependent manner in vivo.

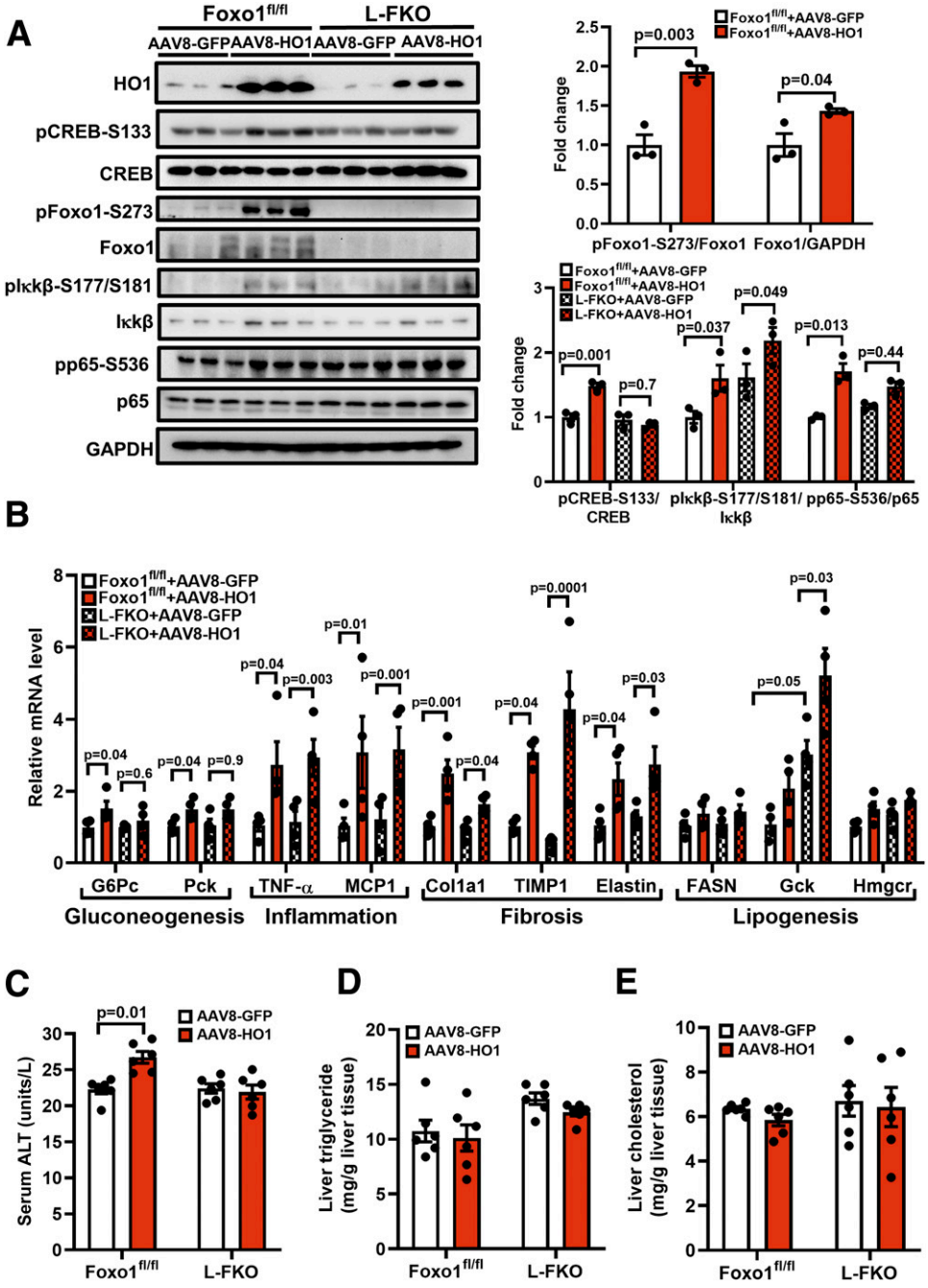

Figure 4— HO1 overexpression in vivo activates NF-κB and Foxo1 in the liver. AAV8-GFP or AAV8-HO1 was delivered via retro-orbital to male mice (8–12 weeks old). Tissues from the mice were collected 14 days after the AAV8 injection. *A*: Total proteins from liver were extracted and loaded onto a 10% SDS-PAGE for Western blotting analyses to detect HO1, pCREB-S133, total CREB, pFoxo1-S273, total Foxo1, pIκkβ-S177/S181, total Iκkβ, pp65-S536, and total p65. The levels of phosphorylated proteins were normalized to the corresponding total protein level. The level of total Foxo1 was normalized to GAPDH. $n = 3$ mice/group. Results are presented as mean ± SEM. *B*: Total RNA from liver tissues were extracted for reverse transcription and quantitative PCR analyses of gluconeogenic, inflammatory, fibrogenic, and lipogenic genes. The relative mRNA level was normalized to cyclophilin. $n = 4$ mice/group. Results are presented as mean ± SEM. *C–E*: Blood samples from the mice were collected for the analysis of ALT activity, and liver tissues were collected for the analyses of triglyceride and cholesterol levels using commercial kits. $n = 6$ mice/group. Results are presented as mean ± SEM.

Since NF-κB signaling might be a potential linkage between HO1 and HGP, we investigated the effects of HO1 overexpression on the NF-κB pathway in the liver tissues. We found that HO1 overexpression showed a pronounced effect in upregulating pp65-S536 (1.71-fold) in the control mice, but its effect in the L-FKO mice was too moderate to be statistically significant (Fig. 4*A*).

Of note, HO1 overexpression also improved the phosphorylation of Iκkβ, which is an upstream regulator of p65 in both L-FKO mice (2.19-fold) and the floxed littermates (1.60-fold) (Fig. 4*A*). The mRNA levels of TNF-α and MCP1, which are p65-targeting proinflammatory genes, were significantly increased by HO1 overexpression in both control and L-FKO mice (Fig. 4*B*).

In addition, HO1 overexpression significantly increased the mRNA levels of fibrogenesis markers, including Col1a1, TIMP1, and elastin (Fig. 4*B*), in the liver of both control and L-FKO mice, indicating a pivotal role of HO1 in promoting hepatic fibrosis. However, HO1 overexpression only increased serum ALT activity in control mice but not the L-FKO mice (Fig. 4*C*). These results suggest the role of hepatic HO1 in facilitating fibrosis and liver injury, which is, at least partially, associated with Foxo1. Although we also examined the effect of HO1 overexpression on lipid metabolism in both control and L-FKO mice, HO1 overexpression barely affected liver triglyceride and cholesterol levels (Fig. 4*D* and *E*). In line with our previous findings, hepatic Foxo1 ablation increased the mRNA level of Gck (17), which was further enhanced by HO1 overexpression (Fig. 4*B*). However, there was no significant effect of HO1 overexpression on the transcriptional levels of other lipogenesis genes, including FASN and Hmgcr (Fig. 4*B*). Collectively, HO1 overexpression in vivo promotes hepatic gluconeogenesis and fibrosis, with a mild effect on lipid metabolism.

HO1 Overexpression Activates Hepatic NF-κB and Foxo1 via Induction of Ferrous Iron Generation

Although a previous study associated the mitigation of insulin resistance in liver-specific HO1 knockout mice with increased hepatic SOD activity (15), the principal function of HO1 is to catalyze the degradation of heme into ferrous iron. Thus, we hypothesized that HO1 overexpression activates hepatic NF-κB and Foxo1 by enhancing the intracellular oxidative stress or/and generating ferrous iron. Surprisingly, HO1 overexpression showed an insignificant effect on both the SOD activity and the ROS production in hepatocytes (Supplementary Fig. 3*A* and *B*). In addition, mRNA levels of Nrf2-targeting ROS detoxification genes were not altered by HO1 overexpression in vivo (Supplementary Fig. 3*C*). By contrast, transfection of Adv-HO1 to hepatocytes for 24 h robustly increased the amount of intracellular ferrous iron, and this effect was abolished by the treatment of iron chelator DFO (Fig. 5*A*). The induction of ferrous iron generation by HO1 overexpression was also evident by the increased amount of ferrous iron accumulated in the AAV8-HO1 liver tissues in both control and L-FKO mice (Fig. 5*B*).

In addition, we found that the chelation of ferrous iron in hepatocytes suppressed the HO1-induced HGP by 11.2% ($P = 0.04$) (Fig. 5*C*). In line with this observation, pretreatment with DFO was found to abolish the activations of NF-κB and Foxo1 in hepatocytes; this was demonstrated by the reduced levels of pIκkβ-S177/S181, pp65-S536, pFoxo1-S273, and total Foxo1 protein abundance (Fig. 5*D*). The suppressive effects of DFO on NF-κB and Foxo1 further contributed to the normalizations of mRNA levels of G6Pc and Pck (Fig. 5*E*).

To determine the essential role of the HO1-induced ferrous iron in promoting the interaction between NF-κB and Foxo1 in hepatocytes, we performed an immunoprecipitation. Foxo1 could be detected in the immunoprecipitates of Iκkβ, which were substantially enhanced by the HO1 overexpression. Such an effect was abolished by the addition of iron chelator DFO (Fig. 5*F*). In summary, HO1 overexpression enhances the generation of ferrous iron in hepatocytes, which triggers the activations of NF-κB and Foxo1 to promote HGP.

HO1 Knockdown Normalizes Gluconeogenesis in L-DKO Mice

It was previously reported that genetically induced insulin-resistant L-DKO mice (with hepatic deletions of IRS1 and IRS2) showed a phenotype of enhanced fasting blood glucose as well as protein abundance of hepatic HO1 (16,25). Therefore, we used AAV8 expressing scramble or HO1 shRNA to determine whether HO1 plays a role in promoting gluconeogenesis under insulin resistance. We found that HO1 knockdown reduced the fasting blood glucose by 22.6% ($P = 0.03$) (Fig. 6*A*) and significantly improved gluconeogenesis during pyruvate tolerance test in L-DKO mice, but the effect in the control mice was mild (Fig. 6*B*). Of note, the knockdown of HO1 also improved glucose tolerance in L-DKO mice (Fig. 6*C*), which was consistent with a previous observation in high-fat diet–fed mice (15). In agreement with the changes in blood glucose, as compared with the control liver, L-DKO liver showed a 54.3% increase in ferrous iron content ($P = 0.03$), which was normalized by HO1 knockdown (Fig. 6*D*); this further suggested the roles of HO1 and associated ferrous iron in enhancing gluconeogenesis.

In line with a previous report (16), there was a 1.35-fold increase in hepatic HO1 protein level in L-DKO mice, as compared with the control mice (Fig. 6*E*). The enhanced phosphorylation of pCREB-S133 (1.48-fold) and pFoxo1-S273 (2.54-fold) in L-DKO mice was normalized by HO1 knockdown (Fig. 6*D*), which contributed to the deactivations of G6Pc and Pck transcripts (Fig. 6*F*). The inhibition of Foxo1 signaling in L-DKO mice by HO1 knockdown was associated with the suppression of NF-κB signaling, which was evident by the reductions of pIκkβ-S177/S181 (from 1.86-fold to 1.26-fold) and pp65-S536 (from 1.62-fold to 0.98-fold) (Fig. 6*E*). The inhibition of NF-κB signaling also contributed to a decrease in the mRNA level of proinflammatory genes, such as IL-6 and TNF-α (Fig. 6*F*). Since HO1-mediated disruption of hepatic mitochondrial function was considered as a pathological mechanism in L-DKO mice (16), we found in this study that the suppressed

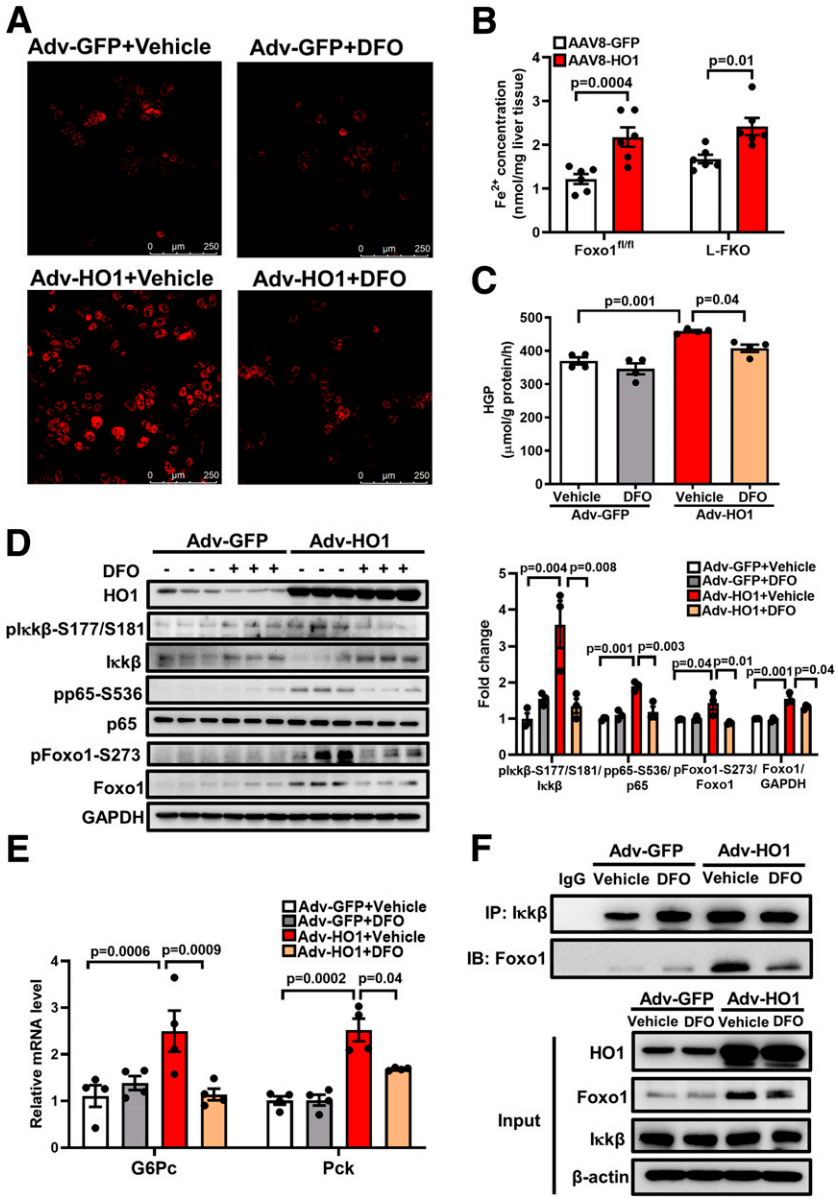

Figure 5—HO1 overexpression activates hepatic NF-κB and Foxo1 by generating ferrous iron. *A*: Hepatocytes from wild-type mice were isolated and transfected with Adv-GFP or Adv-HO1 for 22 h and then treated with 40 μmol/L DFO for 2 h. The FeRhoNox-1 probe was used to detect the intracellular ferrous iron, which was visualized by confocal microscope. *B*: AAV8-GFP or AAV8-HO1 was delivered via retro-orbital to male mice (8–12 weeks old). Tissues from the mice were collected 14 days after the AAV8 injection. The concentration of ferrous iron in the liver tissue was measured and normalized by the weight of liver used for the assessment. $n = 6$ mice/group. Results are presented as mean ± SEM. *C*: Hepatocytes from wild-type mice were isolated. The cells were pretreated with 40 μmol/L DFO for 0.5 h and then transfected with Adv-GFP or Adv-HO1 for 20 h. Afterward, the cells were switched to HGP buffer for 3 h. HGP was normalized to total protein levels. $n = 4$/group. Results are presented as mean ± SEM. *D*: Hepatocytes from wild-type mice were isolated. The cells were pretreated with 40 μmol/L DFO for 0.5 h and then transfected with Adv-GFP or Adv-HO1 for 20 h. The cell lysates were loaded onto a 10% SDS-PAGE for Western blotting analyses to detect HO1, pIκkβ-S177/S181, total Iκkβ, pp65-S536, total p65, pFoxo1-S273, and total Foxo1. The levels of phosphorylated proteins were normalized to the corresponding total protein level. The level of total Foxo1 was normalized to GAPDH. $n = 3$/group. Results are presented as mean ± SEM. *E*: Hepatocytes from wild-type mice were isolated. The cells were pretreated with 40 μmol/L DFO for 0.5 h and then transfected with Adv-GFP or Adv-HO1 for 24 h. The RNA was extracted and expression of G6Pc and Pck determined by quantitative PCR. The cellular protein lysates from *E* were used for immunoprecipitation of Iκkβ. *F*: The immunoprecipitation (IP) complex and the cell lysates (input) were loaded onto a 10% SDS-PAGE for Western blotting analyses. IB, immunoblotting.

mRNA levels of QUCRC1 and MT-CO1 were restored by HO1 knockdown in DKO liver (Fig. 6*F*), which is an indicative of rescued heme-dependent electron transport chain complex III and complex IV (20). The rescued hepatic mitochondrial function by HO1 knockdown in DKO liver was also evident by the restored mRNA level of genes responsible for fatty acid oxidation, including Hadha, Cpt1a, and VLCAD (Fig. 6*F*).

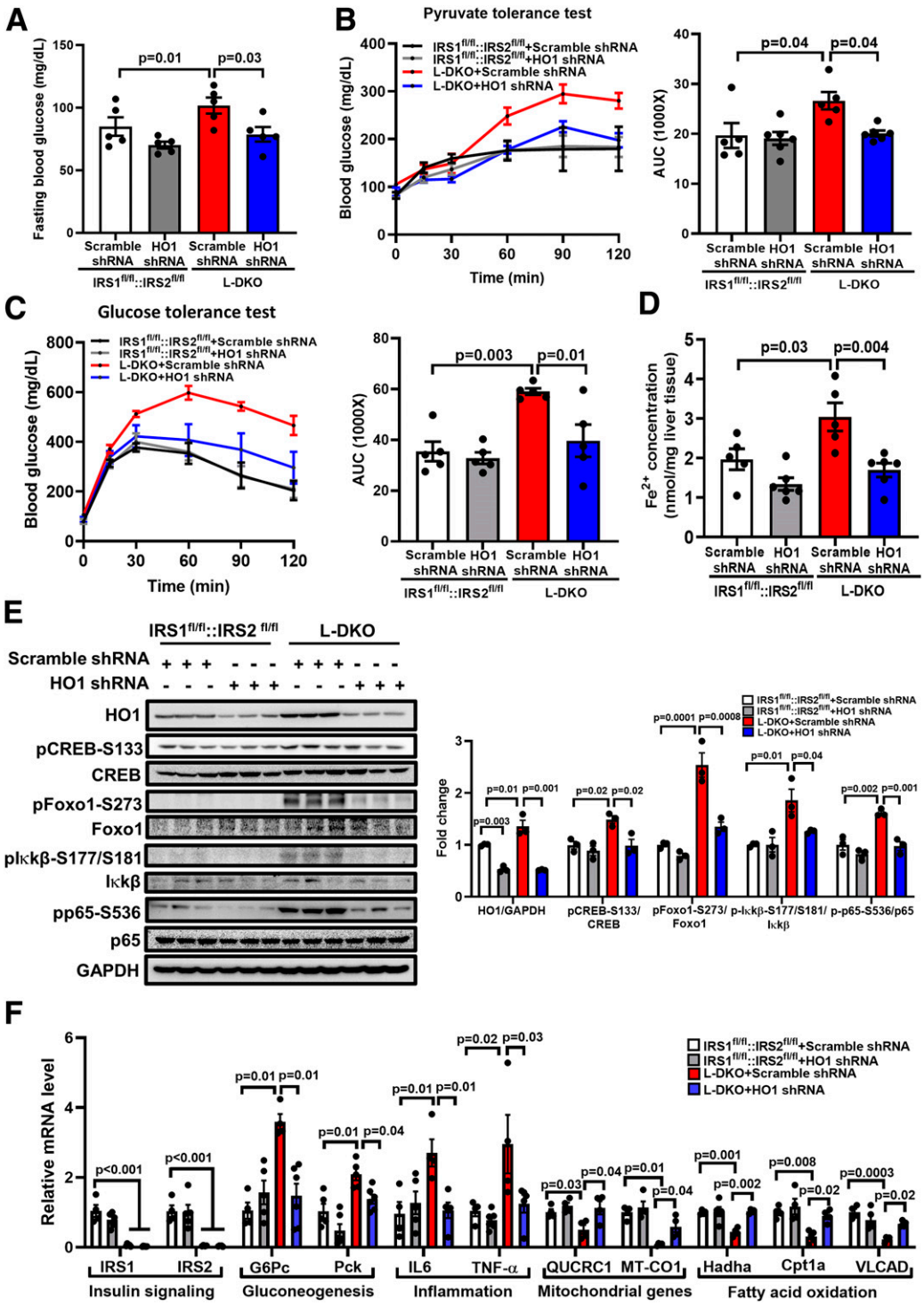

Figure 6—HO1 knockdown normalizes gluconeogenesis in L-DKO mice. AAV-based scramble or HO1 shRNA was delivered to 8- to 12-week-old male IRS1$^{fl/fl}$::IRS2$^{fl/fl}$ or L-DKO mice via retro-orbital. *A*: Blood glucose after 16 h of fasting or underfeeding conditions was measured 8 days after the injection. n = 5–6 mice/group. Results are presented as mean ± SEM. *B* and *C*: The mice were fasted for 16 h and then subjected to a 2-h pyruvate tolerance test (8 days postinjection, 2 g/kg body weight pyruvate i.p. injection) or glucose tolerance test (11 days postinjection of virus, 2 g/kg body weight glucose i.p. injection). The area under the curve (AUC) of each profile was calculated. n = 5–6 mice/group. Results are presented as mean ± SEM. *D*: The concentration of ferrous iron in the liver tissue was measured and normalized by the weight of liver used for the assessment. n = 6 mice/group. Results are presented as mean ± SEM. *E*: Liver tissues of the mice were collected 14 days after the AAV8 shRNA injection. Total proteins from liver were extracted and loaded onto a 10% SDS-PAGE for Western blotting analyses to detect HO1, pCREB-S133, total CREB, pFoxo1-S273, total Foxo1, pIκkβ-S177/S181, total Iκkβ, pp65-S536, and total p65. The levels of phosphorylated proteins were normalized to the corresponding total protein level. The level of total Foxo1 was normalized to GAPDH. n = 3 mice/group. Results are presented as mean ± SEM. *F*: Total RNA from liver tissues were extracted for reverse transcription and quantitative PCR analyses to assess the mRNA levels of IRS1, IRS2, and genes related to gluconeogenesis, inflammation, and fatty acid oxidation. The relative mRNA level was normalized to cyclophilin. n = 4–5 mice/group. Results are presented as mean ± SEM.

Hepatic Iron Status Regulates Gluconeogenesis

It has been reported that iron-dextran induced systemic iron overload, resulting in insulin resistance in skeletal muscle via inhibiting autophagic flux (22). In addition, feeding of a high-iron diet increased fasting blood glucose in low-fat diet–fed, high-fat diet–fed, and *db/db* mice (26,27), but the underlying mechanisms remain elusive. Hereby, we injected iron-dextran to induce iron overload in control and L-FKO mice to further investigate the role of hepatic iron status in regulating gluconeogenesis and the involvement of Foxo1. It was found that intravenous injections of iron-dextran significantly increased fasting blood glucose in the control mice (82.6 mg/dL vs. 105.4 mg/dL, $P = 0.02$), but the effect was absent in the L-FKO mice (Fig. 7*A*). Iron-dextran injections also impaired pyruvate tolerance in control mice but not in the L-FKO mice (Fig. 7*B*). These data suggest that iron-dextran promotes hepatic gluconeogenesis via Foxo1.

Iron-dextran–induced iron overload increased the amounts of total iron and ferrous iron in the liver of both control and L-FKO mice (Fig. 7*C* and *D*). However, serum glucagon concentration was unaffected by the iron-dextran injection (Fig. 7*E*), which indicates that hepatic iron overload promotes gluconeogenesis without affecting glucagon secretion. By contrast, the hepatic PKA→Foxo1 axis was activated by the injection of iron-dextran, which was evident by the 1.2-fold, 1.7-fold, and 1.6-fold increase of pFoxo1-S273, total Foxo1, and pCREB-S133, respectively, in the control liver (Fig. 7*F*). Of note, the injection of iron-dextran increased the level of pIκkβ-S177/S181 in both control (1.6-fold) and L-FKO liver (1.9-fold) (Fig. 7*F*). Collectively, hepatic iron overload activates Iκkβ and the PKA→Foxo1 axis to promote gluconeogenesis.

Finally, we injected iron chelator DFO into the insulin-resistant L-DKO mice to further examine whether iron chelation could rescue the aberrant gluconeogenesis. Of note, the treatment of iron chelator DFO significantly reduced fasting blood glucose by 26.6% in L-DKO mice (Fig. 7*G*). The response to pyruvate challenge in L-DKO mice was also normalized by DFO injection (Fig. 7*H*). These results suggested that the mitigation of HO1-associated hepatic iron overload contributes to suppressing gluconeogenesis under insulin-resistant conditions. However, the treatment of DFO barely affected the fasting blood glucose and pyruvate tolerance test profile under normal physiological conditions (Fig. 7*G* and *H*, $IRS1^{fl/fl}$::$IRS2^{fl/fl}$ + vehicle vs. $IRS1^{fl/fl}$::$IRS2^{fl/fl}$ + DFO). The differential regulatory roles of DFO in control and L-DKO mice indicated that the ferrous iron chelated under normal conditions might be compensated by other mechanisms. Conversely, the chelation of excessive ferrous iron, which is associated with HO1 upregulation, is beneficial for mitigating hyperglycemia in insulin-resistant mice. Overall, all of the above data indicate that iron overload or chelation in mice recapitulates the key aspects of hepatic iron in control of gluconeogenesis via Foxo1.

DISCUSSION

Despite the protective effects in various organs reported for HO1 (28), we and other groups demonstrated the detrimental roles of HO1 in disrupting hepatic mitochondrial function (16) and driving insulin resistance in mouse and humans (15); this impelled us to further identify the multifaceted roles of HO1 in hepatic glucose metabolism. In the current study, we demonstrated that *1*) HO1 overexpression promotes gluconeogenesis via Foxo1, which occurs through Foxo1-S273 phosphorylation; *2*) overexpression of HO1 activates NF-κB by generating excessive ferrous iron; and *3*) suppression of HO1 rescues gluconeogenesis under insulin resistance, such as in L-DKO mice. Our results provided solid biochemical evidence for the roles of HO1 involved in hepatic glucose homeostasis.

HO1 is considered as a Foxo1-targeting gene, as it contains a Foxo1 recognition motif, TATTTT (10). The Foxo1-regulated HO1 plays a pivotal role in the hepatic mitochondrial functions under insulin resistance; this was demonstrated by the mitochondrial dysfunction present in the liver of the insulin-resistant L-DKO mice, while the mitochondrial function was restored in the L-TKO mice (L-DKO mice with the deletion of Foxo1) (16). In this study, we report the reversible regulation of Foxo1 by HO1 to promote gluconeogenesis, which reveals a novel relationship between Foxo1 and HO1. Importantly, we also found that HO1 enhances HGP by activating the PKA→Foxo1 axis, specifically by increasing the phosphorylation of Foxo1 at Ser273 (equivalent to Ser276 in humans), which is a site we previously identified to be regulated by glucagon signaling (6). This finding further proves the essential role of the PKA→Foxo1 axis in gluconeogenesis, which can be targeted by different signaling cascades.

Our studies indicate that the activation of NF-κB by HO1 overexpression in hepatocytes promotes gluconeogenesis via PKA. It was reported that deletion of p65 gene in hepatocytes contributed to a weak response during the pyruvate tolerance test, as well as reduced levels of PKA activity and gluconeogenic gene transcriptions; this was considered to be regulated by cyclic nucleotide phosphodiesterase-3B (24). Thus, we speculate that the PKA→Foxo1 axis is downstream of phosphodiesterase-3B. However, we cannot rule out the possibility of other important factors to bridge NF-κB and Foxo1 since Foxo1 can be regulated by multiple kinases (29–32). Of note, it was reported that Iκk can directly phosphorylate Foxo3a at Ser644 (a site that is independent of Akt regulation) in human breast cancer cells, which promotes Foxo3a ubiquitination and degradation (33). Thus, it is also possible that Iκk may directly interact with Foxo1 to promote gluconeogenesis, and the Iκk-regulated phosphorylation sites of Foxo1 are unknown and worth being characterized in future studies.

In the current study, we showed the pivotal role of HO1-induced ferrous iron in activating NF-κB and PKA→Foxo1-S273 to promote gluconeogenesis. Indeed, the activation of NF-κB by ferrous iron has been reported in

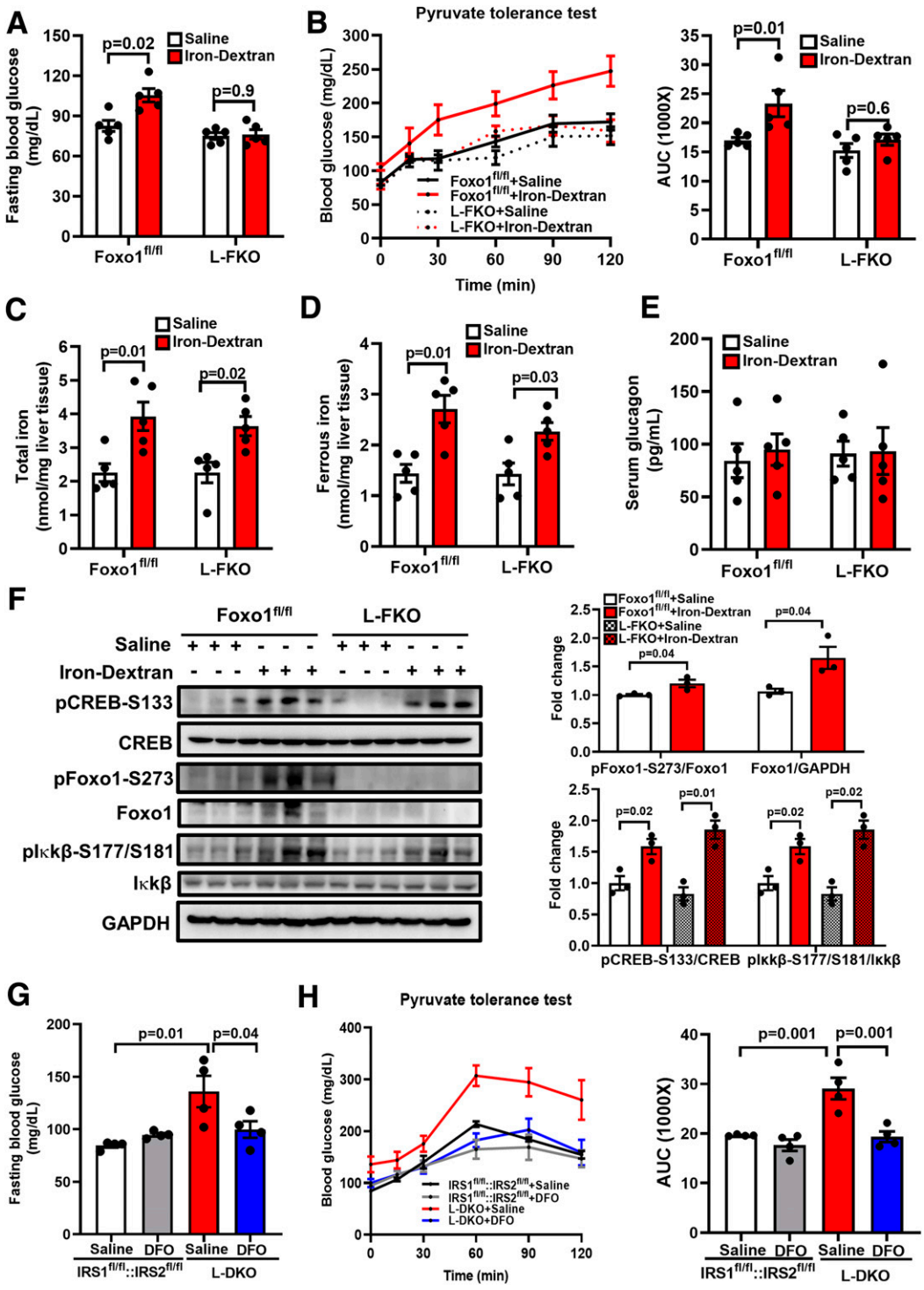

Figure 7—Hepatic iron status regulates gluconeogenesis. The 8- to 12-week-old Foxo1$^{fl/fl}$ or L-FKO male mice were injected with saline or iron-dextran (22.5 mg/kg body weight) intravenously twice at intervals of 4 h. *A* and *B*: Fasting blood glucose was measured 24 h after the first injection of iron-dextran upon 16-h fasting, followed by a 2-h pyruvate tolerance test (2 g/kg body weight pyruvate i.p. injection). The area under the curve (AUC) of each profile was calculated. $n = 5$ mice/group. Results are presented as mean ± SEM. *C–E*: Liver and blood samples were collected after 24 h of the first injection of iron-dextran upon 16-h fasting. The contents of total iron and ferrous iron in the liver as well as the serum glucagon level were measured by commercially available kits. $n = 5$ mice/group. Results are presented as mean ± SEM. *F*: Liver samples were collected 24 h after the first injection of iron-dextran upon 16-h fasting. Total proteins from the liver were extracted and loaded onto a 10% SDS-PAGE for Western blotting analyses to detect pCREB-S133, total CREB, pFoxo1-S273, total Foxo1, pIκkβ-S177/S181, and total Iκkβ. The levels of phosphorylated proteins were normalized to the corresponding total protein level. The level of total Foxo1 was normalized to GAPDH. $n = 3$ mice/group. Results are presented as mean ± SEM. *G* and *H*: Male (8–12 weeks old) IRS1$^{fl/fl}$::IRS2$^{fl/fl}$ or L-DKO mice were treated with 10 mg/kg body weight DFO by i.p. injection and then fasted for 14 h, followed by a second injection of DFO with the same dosage. The fasting blood glucose was measured, and a pyruvate tolerance test (2 g/kg body weight pyruvate i.p. injection) was performed 2 h after the second injection of DFO. $n = 4$ mice/group. Results are presented as mean ± SEM.

hepatic macrophages, which was considered to be involved in the pathogenesis of alcoholic liver injury (34–36). Our findings from this study further broaden the pivotal role of ferrous iron–activated NF-κB in the liver, which is associated with glucose production. Although the causal relationship between iron overload and metabolic dysfunction has been recognized in the liver, skeletal muscle, and adipose tissue (22,37–40), the underlying mechanism as well as the origin of iron accumulation remain elusive. Our findings in this study shed a new insight on the role of HO1 in the development of hepatic iron overload and subsequent disruption of hepatic glucose homeostasis, which is controlled by Foxo1.

The pathological effects of ferrous iron have been recently addressed in other cells, such as cardiomyopathy, which occurs through the induction of ferroptosis in cardiomyocytes (41). In this study, we identified the role of HO1 and the associated ferrous iron accumulation in the liver involving in glucose metabolism. It would be of interest to further investigate the effects on hepatocytes ferroptosis and associated liver diseases of a constitutive activation of HO1 and generation of ferrous iron in the liver in transgenic mouse models.

In this study, we found that in the insulin-resistant L-DKO mice, the levels of HO1 and ferrous iron in the liver were higher than that of control littermates; this suggests that the upregulation of HO1 and the consequent accumulation of hepatic ferrous iron may serve as a key mechanism for hyperglycemia in L-DKO mice. As documented, the treatment of iron chelator DFO improved the adipocyte dysfunction and systemic insulin resistance in diabetic mice models (42–44). In agreement with these reports, we found that either HO1 knockdown or iron chelation reduced the fasting blood glucose and improved pyruvate tolerance test profile in L-DKO mice; this indicates that suppressing HO1 or chelating the excessive ferrous iron in the liver may be an alternative strategy for mitigating hyperglycemia under insulin resistance, which is accomplished through the suppression of gluconeogenesis. Of note is that HO1 knockdown also improved expression of genes responsible for mitochondrial function and fatty acid oxidation in the liver of insulin-resistant mice.

In summary, our study demonstrates the role of hepatic HO1 in promotion of gluconeogenesis via Foxo1 (Fig. 8), which further supports the notion that HO1 may have detrimental effects in the liver on disrupting glucose homeostasis. Previous studies have concluded that the reduced bioavailability of heme, which is degraded by HO1, results in hepatic mitochondrial dysfunction and insulin resistance (15,16). In the current study, we identified that the HO1-mediated ferrous iron production is a pivotal player in promoting HGP, which unveils a novel mechanism of HO1 involving in liver metabolism. Thus, HO1 inhibition, instead of activation, can be a strategy for the management of T2D in the future.

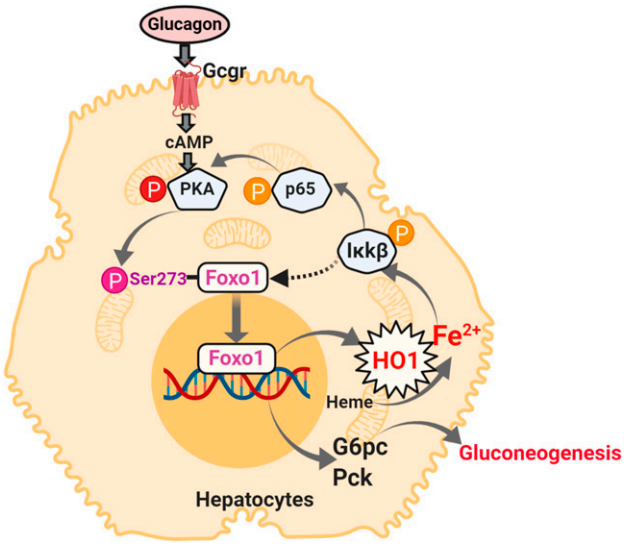

Figure 8—Schematic diagram represents the role of HO1 in regulating gluconeogenesis. HO1 overexpression produces excessive ferrous iron, which activates NF-κB in hepatocytes. As a consequence, Foxo1 is phosphorylated at Ser273, which activates the transcriptions of genes encoding for gluconeogenic enzymes. The figure was created with BioRender.com.

Acknowledgments. The authors thank Mike Honig (Houston, TX), who provided English editing for the manuscript.

Funding. This work was supported by National Institutes of Health grants (R01 DK095118 and R01 DK120968), an American Diabetes Association Career Development Award (1-15-CD-09), faculty startup funds from Texas A&M University Health Science Center and AgriLife Research, and a U.S. Department of Agriculture National Institute of Food and Agriculture grant (Hatch 1010958) to S.G. (principal investigator). S.G. is the recipient of the 2015 American Diabetes Association Research Excellence Thomas R. Lee Career Development Award. This work was also partially supported by National Institutes of Health grants R01DK118334 and R01AG064869 to Y.S. (principal investigator) and S.G. (co-investigator).

Duality of Interest. No potential conflicts of interest relevant to this article were reported.

Author Contributions. W.L., W.Y., and S.G. designed experiments. W.L. and W.Y. conducted experiments and performed data analyses. W.L. and S.G. wrote the manuscript. W.Y., Z.S., W.A., Q.P., Y.S., and S.G. reviewed and edited the manuscript. S.G. supervised the project, conceived the hypothesis, and designed experiments. S.G. is the guarantor of this work and, as such, had full access to all the data in the study and takes responsibility for the integrity of the data and the accuracy of the data analysis.

Prior Presentation. Parts of this study were presented in abstract form at the 80th Scientific Sessions of the American Diabetes Association, 12–16 June 2020.

References

1. Gromada J, Duttaroy A, Rorsman P. The insulin receptor talks to glucagon? Cell Metab 2009;9:303–305

2. Edgerton DS, Cherrington AD. Glucagon as a critical factor in the pathology of diabetes. Diabetes 2011;60:377–380

3. Accili D, Arden KC. FoxOs at the crossroads of cellular metabolism, differentiation, and transformation. Cell 2004;117:421–426

4. Unger RH. Glucagon physiology and pathophysiology. N Engl J Med 1971; 285:443–449

5. Rena G, Guo S, Cichy SC, Unterman TG, Cohen P. Phosphorylation of the transcription factor forkhead family member FKHR by protein kinase B. J Biol Chem 1999;274:17179–17183
6. Wu Y, Pan Q, Yan H, et al. Novel mechanism of Foxo1 phosphorylation in glucagon signaling in control of glucose homeostasis. Diabetes 2018;67:2167–2182
7. Kitamura T. The role of FOXO1 in β-cell failure and type 2 diabetes mellitus. Nat Rev Endocrinol 2013;9:615–623
8. Xin Z, Ma Z, Hu W, et al. FOXO1/3: potential suppressors of fibrosis. Ageing Res Rev 2018;41:42–52
9. Matsumoto M, Han S, Kitamura T, Accili D. Dual role of transcription factor FoxO1 in controlling hepatic insulin sensitivity and lipid metabolism. J Clin Invest 2006;116:2464–2472
10. Alam J, Cai J, Smith A. Isolation and characterization of the mouse heme oxygenase-1 gene. Distal 5′ sequences are required for induction by heme or heavy metals. J Biol Chem 1994;269:1001–1009
11. Abraham NG, Kappas A. Pharmacological and clinical aspects of heme oxygenase. Pharmacol Rev 2008;60:79–127
12. Alam J, Stewart D, Touchard C, Boinapally S, Choi AMK, Cook JL. Nrf2, a Cap'n'Collar transcription factor, regulates induction of the heme oxygenase-1 gene. J Biol Chem 1999;274:26071–26078
13. Ndisang JF, Lane N, Jadhav A. Upregulation of the heme oxygenase system ameliorates postprandial and fasting hyperglycemia in type 2 diabetes. Am J Physiol Endocrinol Metab 2009;296:E1029–E1041
14. Huang J-Y, Chiang M-T, Chau L-Y. Adipose overexpression of heme oxygenase-1 does not protect against high fat diet-induced insulin resistance in mice. PLoS One 2013;8:e55369
15. Jais A, Einwallner E, Sharif O, et al. Heme oxygenase-1 drives metaflammation and insulin resistance in mouse and man. Cell 2014;158:25–40
16. Cheng Z, Guo S, Copps K, et al. Foxo1 integrates insulin signaling with mitochondrial function in the liver. Nat Med 2009;15:1307–1311
17. Zhang K, Li L, Qi Y, et al. Hepatic suppression of Foxo1 and Foxo3 causes hypoglycemia and hyperlipidemia in mice. Endocrinology 2012;153:631–646
18. Guo S, Copps KD, Dong X, et al. The Irs1 branch of the insulin signaling cascade plays a dominant role in hepatic nutrient homeostasis. Mol Cell Biol 2009;29:5070–5083
19. Yan H, Yang W, Zhou F, et al. Estrogen improves insulin sensitivity and suppresses gluconeogenesis via the transcription factor Foxo1. Diabetes 2019;68:291–304
20. Yang W, Yan H, Pan Q, et al. Glucagon regulates hepatic mitochondrial function and biogenesis through FOXO1. J Endocrinol 2019;241:265–278
21. Hassannia B, Wiernicki B, Ingold I, et al. Nano-targeted induction of dual ferroptotic mechanisms eradicates high-risk neuroblastoma. J Clin Invest 2018;128:3341–3355
22. Jahng JWS, Alsaadi RM, Palanivel R, et al. Iron overload inhibits late stage autophagic flux leading to insulin resistance. EMBO Rep 2019;20:e47911
23. Wang S, Liu C, Pan S, et al. Deferoxamine attenuates lipopolysaccharide-induced inflammatory responses and protects against endotoxic shock in mice. Biochem Biophys Res Commun 2015;465:305–311
24. Ke B, Zhao Z, Ye X, et al. Inactivation of NF-κB p65 (RelA) in liver improves insulin sensitivity and inhibits cAMP/PKA pathway. Diabetes 2015;64:3355–3362
25. Dong XC, Copps KD, Guo S, et al. Inactivation of hepatic Foxo1 by insulin signaling is required for adaptive nutrient homeostasis and endocrine growth regulation. Cell Metab 2008;8:65–76
26. Choi JS, Koh I-U, Lee HJ, Kim WH, Song J. Effects of excess dietary iron and fat on glucose and lipid metabolism. J Nutr Biochem 2013;24:1634–1644
27. Ma W, Feng Y, Jia L, et al. Dietary iron modulates glucose and lipid homeostasis in diabetic mice. Biol Trace Elem Res 2019;189:194–200
28. Soares MP, Bach FH. Heme oxygenase-1: from biology to therapeutic potential. Trends Mol Med 2009;15:50–58
29. Guo S. Insulin signaling, resistance, and the metabolic syndrome: insights from mouse models into disease mechanisms. J Endocrinol 2014;220:T1–T23
30. Ozcan L, Wong CC, Li G, et al. Calcium signaling through CaMKII regulates hepatic glucose production in fasting and obesity. Cell Metab 2012;15:739–751
31. Asada S, Daitoku H, Matsuzaki H, et al. Mitogen-activated protein kinases, Erk and p38, phosphorylate and regulate Foxo1. Cell Signal 2007;19:519–527
32. Cao W, Collins QF, Becker TC, et al. p38 Mitogen-activated protein kinase plays a stimulatory role in hepatic gluconeogenesis. J Biol Chem 2005;280:42731–42737
33. Hu MCT, Lee D-F, Xia W, et al. IkappaB kinase promotes tumorigenesis through inhibition of forkhead FOXO3a. Cell 2004;117:225–237
34. Tsukamoto H. Iron regulation of hepatic macrophage TNFalpha expression. *Free Radic Biol Med* 2002;32:309–313
35. Xiong S, She H, Takeuchi H, et al. Signaling role of intracellular iron in NF-kappaB activation. J Biol Chem 2003;278:17646–17654
36. Tsukamoto H, Lin M, Ohata M, Giulivi C, French SW, Brittenham G. Iron primes hepatic macrophages for NF-kappaB activation in alcoholic liver injury. Am J Physiol 1999;277:G1240–G1250
37. Datz C, Felder TK, Niederseer D, Aigner E. Iron homeostasis in the metabolic syndrome. Eur J Clin Invest 2013;43:215–224
38. Fernández-Real JM, López-Bermejo A, Ricart W. Cross-talk between iron metabolism and diabetes. Diabetes 2002;51:2348–2354
39. Milic S, Mikolasevic I, Orlic L, et al. The role of iron and iron overload in chronic liver disease. Med Sci Monit 2016;22:2144–2151
40. Dongiovanni P, Ruscica M, Rametta R, et al. Dietary iron overload induces visceral adipose tissue insulin resistance. Am J Pathol 2013;182:2254–2263
41. Fang X, Wang H, Han D, et al. Ferroptosis as a target for protection against cardiomyopathy. Proc Natl Acad Sci U S A 2019;116:2672–2680
42. Yan H-F, Liu Z-Y, Guan Z-A, Guo C. Deferoxamine ameliorates adipocyte dysfunction by modulating iron metabolism in ob/ob mice. Endocr Connect 2018;7:604–616
43. Tajima S, Ikeda Y, Sawada K, et al. Iron reduction by deferoxamine leads to amelioration of adiposity via the regulation of oxidative stress and inflammation in obese and type 2 diabetes KKAy mice. Am J Physiol Endocrinol Metab 2012;302:E77–E86
44. Cooksey RC, Jones D, Gabrielsen S, et al. Dietary iron restriction or iron chelation protects from diabetes and loss of β-cell function in the obese (ob/ob lep-/-) mouse. Am J Physiol Endocrinol Metab 2010;298:E1236–E1243